HHS Public Access

Author manuscript

Soft Matter. Author manuscript; available in PMC 2016 November 28.

Published in final edited form as:

Soft Matter. 2015 November 28; 11(44): 8621–8631. doi:10.1039/c5sm01778e.

Characterization and Control of Surfactant-Mediated Norovirus Interactions

Brittany S. Mertens and **Orlin D. Velev***

Department of Chemical and Biomolecular Engineering, North Carolina State University, Raleigh, NC 27695-7905, USA

Abstract

Understanding of the colloidal interactions of Norovirus particles in aqueous medium could provide insights on the origins of the notorious stability and infectivity of these widespread viral agents. We characterized the effects of solution pH and surfactant type and concentration on the aggregation, dispersion, and disassembly of Norovirus virus-like particles (VLPs) using dynamic light scattering, electrophoretic light scattering, and transmission electron microscopy. Owing to net negative surface charge of the VLPs at neutral pH, low concentrations of cationic surfactant tend to aggregate the VLPs, whereas low concentrations of anionic surfactant tend to disperse the particles. Increasing the concentration of these surfactants beyond their critical micelle concentration leads to virus capsid disassembly and breakdown of aggregates. Non-ionic surfactants, however, had little effect on virus interactions and likely stabilized them additionally in suspension. The data were interpreted on the basis of simple models for surfactant binding and re-charging of the virus capsid. We used zeta potential data to characterize virus surface charge and interpret the mechanisms behind these demonstrated surfactant-virus interactions. The fundamental understanding and control of these interactions will aid in practical formulations for virus inactivation and removal from contaminated surfaces.

Introduction

We report and analyze data on the colloidal interactions of Noroviruses as soft nanoparticles in water using common colloidal characterization techniques such as dynamic light scattering (DLS) and transmission electron microscopy (TEM). The colloidal state of virus particles under various conditions is an aspect of virus behavior that complicates disinfection,[1] so we have investigated the behavior of Norovirus-like particles in the presence of different classes of surfactants. Norovirus poses a major threat to public health and is also considered a potential bioterrorism hazard due to the acute and debilitating symptoms of infection.[2] Noroviruses are composed of a protein capsid that encases a single-stranded RNA core. 180 major capsid proteins (VP1) form dimers, which then assemble into a T=3 icosahedron ranging between 30–38 nm in diameter.[3,4] As a gastroenteric virus, Norovirus is stable in nature at a wide range of pH levels and therefore can be present as dispersed particles or aggregates with varying sizes.[5] Norovirus also has astounding persistence with the ability to withstand a wide range of temperatures, pH levels, and

* odvelev@ncsu.edu.

chemical treatments in the environment.[6] It can remain on dry surfaces for weeks without losing significant infectivity.[7] Because of the extreme resistance properties that Noroviruses possess, they fail to respond to neutralizing methods effective against most other pathogens.[8–11] Norovirus requires more potent disinfection strategies and longer contact times in comparison to other foodborne pathogens.[12] Studies have shown that virus aggregates help sustain and may even enhance infectivity by shielding viruses on the inside of aggregates from virucidal treatments.[13,14] Virus aggregation at different pH values and ionic strengths has been well documented in relation to membrane filtration processes,[15–18] but less research has been conducted to elucidate the impact of surfactant type and concentration on virus particle aggregation and subsequent deactivation.[19–21]

Virus-like particles (VLPs) are a useful alternative to viable Noroviruses for studying particle surface properties and interactions.[22,23] During their preparation, Norovirus major capsid protein is produced in a separate expression vector and spontaneously assembles into the virus capsid structure without infectious RNA inside.[3,22] Because the VLPs lack internal RNA that can contribute to particle stability and interactions, VLPs have not been considered as suitable substitutes for viable viruses in disinfection studies.[24] It has been shown that the method used to purify viruses and VLPs also has an impact on virus-virus interactions.[25,26] Instead VLPs may be used as predictors of virus capsid interactions in the presence of differing solution chemistries and possible vaccine agents.[27,28] Norovirus VLPs have been used to study conformational capsid changes that facilitate disassembly over a range of pH levels and temperatures,[23, 29–32] and virus surface charge has been previously shown to govern particle behavior.[33] The assembly and disassembly of Norovirus VLPs has been shown to mostly involve stable protein dimers, intermediates containing about 11 dimers, and complete capsids composed of 90 dimers.[34] The P domain of the major capsid protein, which forms protrusions on the capsid, is involved in the interactions that form stable dimers, and the S domain is involved in the interactions between dimers to form the icosahedral structure.[35] The capsid protrusions may contribute to VLP stability by adding rigidity to the particles.[36]

Because the outermost layer of Norovirus is the protein capsid, its aggregation behavior will have similarities to that of general proteins. Protein interactions are complex and can be influenced by electrostatic double-layer forces, van der Waals forces, hydration, and steric forces.[37] The complexity of protein interactions arises from the characteristic and diverse amino acid compositions that produce hydrophobic, hydrophilic, anionic, and cationic regions on the protein.[38] Slight differences in the sequences of the virus capsid proteins result in perceptible differences in virus susceptibility to certain disinfectants,[39] so understanding virus surface properties is especially important. The factors and interactions related to protein aggregation have been extensively investigated[40] as they have relevance to food processing[41] and drug development and delivery.[42,43] We use this knowledge and similar experimental techniques to characterize virus aggregation and dispersion.[44] Electrostatic interactions in water medium strongly influence general colloidal particle behavior, including that of viruses. Non-enveloped viruses have been extensively modeled as soft, porous colloids[45,46] with three shells of charge density, including the protein capsid, capsid-bound RNA, and free RNA.[47,48] Because of the porosity of some virus capsids, the charge of internal RNA has a significant effect on their apparent isoelectric point and

therefore would also influence virus stability and binding behavior. Capsid porosity complicates the use of zeta potential as a means of describing particle surface charge even in the absence of internal RNA.[47] Here we use zeta potential data to evaluate the effect of surfactant-altered apparent capsid charge on Norovirus capsid aggregation, dispersion, and disassembly.

Naturally-occurring surface-active molecules such as proteins that behave as surfactants[49] and saponins[50] have been shown to exhibit significant bactericidal and virucidal behavior. These surfactants provide motivation to study the interactions between virus particles and various classes of surfactants to elucidate possible mechanisms of deactivation or stabilization. Surfactants concentrated above their critical micelle concentration (CMC) in aqueous solution form micellar aggregates, which can vary depending on the molecular and electrolytic solvent environment. Surfactant binding to folded or unfolded proteins can influence micelle formation by the development of surfactant-protein structures in addition to free micelles.[51,52] Some micelles have the ability to entrap and solubilize other molecules or particles.[53] Bound surfactants can modify the apparent surface charge of nanoparticles[54] and therefore influence the interactions and aggregation of these particles in solution. Because proteins are electrostatically diverse and possess hydrophobic, hydrophilic, anionic, and cationic regions, they can bind both anionic and cationic surfactants strongly. Surfactants with charged head groups can alter the effective surface charge of surfaces or particles by shielding opposite charges or adding charge to a hydrophobic site.[55] The high surface activity of surfactants allows them to dictate protein stability and interactions.

We use Norovirus VLPs as a model system of specific practical relevance to study surfactant-imposed colloidal interactions of virus capsids. These VLPs are from a GII.4 Houston strain (Houston/TCH186/02) of Norovirus that has not yet been characterized by crystallography. The diameter of the VLPs is assumed to be close to that of the GI.1 Norwalk strain, which has been characterized at 38.0 nm in diameter.[3] The intact virus strain contains a genome 7559 base pairs in length and is infectious to humans.[56] We selected one common and widespread anionic, cationic, and nonionic surfactant to represent each surfactant type. We used sodium dodecyl sulfate (SDS) as an anionic surfactant because of its common use in hand soaps, dish detergents, and other household products. We selected cetyltrimethylammonium bromide (CTAB) as a cationic surfactant because of its use as an antimicrobial in many cleaning products. The nonionic surfactant was Tween 20 (polysorbate 20), which is extensively used in many processed food and drink products (which eventually may also be carriers for Noroviruses). For varying concentrations of each of these surfactants, we use DLS to determine the sizes of particles in solution and analyze each peak of intensity distributions to represent either virus aggregates, dispersed viruses, or disassembled virus capsids. We then present electrophoretic light scattering (ELS) data and compare it to the theoretically calculated capsid charges to explain the mechanisms behind each observed colloidal behavior. Finally, we confirm the presence of VLP aggregation, dispersion, and disassembly with TEM images and describe the impact that each behavior makes on virus infectivity, persistence, and disinfection.

Results and discussion

Dynamic light scattering (DLS) characterization of virus aggregation state at varying pH

We used DLS to measure the size of particles present in VLP suspensions in phosphate-buffered saline (PBS). The VLPs concentration was fixed, while pH, surfactant type, and surfactant concentration were varied. For the surfactant effect studies, SDS, CTAB, and Tween 20 were each added individually at concentrations ranging from 0.01% to 0.5% by weight. All of the suspensions containing surfactant were produced at pH 7.4. These data were used to determine whether the VLPs were aggregated, dispersed, or disassembled at each pH or surfactant concentration. We also used ELS to measure the zeta potential of particles present in VLP suspensions with varying pH and surfactant concentrations below 0.05%. Micelles would interfere with the measurement of VLP zeta potential, so higher surfactant concentrations were excluded. These data were used to correlate the electrostatic properties of the particles with their interactions observed by DLS. Finally, we used TEM to view aggregated, dispersed, or disassembled VLPs under selected surfactant conditions.

DLS data can be represented as intensity, volume, or number distributions of the particle size. We determined that with the concentration of VLPs and surfactants used, the intensity distribution gives an accurate representation of the relative amount of dispersed or aggregated VLPs remaining in solution after each treatment. For the intensity of scattered light, $I \sim r^6$, so a VLP that is 40 nm in diameter will scatter about 90,000 times more light than a micelle or protein that is 6 nm in diameter. For our VLP and surfactant mixtures, all DLS data are presented as plots of the intensity distributions because the concentration of surfactant micelles in solution is high enough to scatter light proportional to the amount scattered by dispersed VLPs or aggregates. Micelles would be the only particles represented in a volume distribution, where $V \sim r^3$. Details of these calculations are presented in Methods. The corresponding DLS correlation function data are presented in the Supplementary Information.

Because the capsid protein dimers are very similar in size to surfactant micelles, the proteins and micelles overlap in the same peak in the intensity distributions. Therefore these peaks cannot be used to determine the relative amounts of capsid protein dimers produced from VLPs by each treatment. Instead we evaluate the presence or absence of peaks attributed to dispersed or aggregated VLPs to determine the efficacy of each additive to disrupt the particles. Also, because most samples in this study are polydisperse, the algorithms used by the DLS software to determine exact particle size are not precise. The same particle may be reported by the software as slightly different in size in separate measurements. We therefore use ranges of particle sizes to define three categories of peaks in the DLS distributions presented here. A peak in the region of 5–10 nm most likely arises from surfactant micelles, capsid protein dimers, or both; a peak in the region of 30–70 nm represents disperse VLPs; and a peak above 100 nm indicates the presence of VLP aggregates. The data shown in Fig. 1 demonstrate that the VLPs are well dispersed at low and high pH, while aggregation is prevalent at pH values close to the isoelectric point of the capsid proteins (pH~4.5). Some aggregation is present at neutral pH due to lower magnitude of surface charge compared to low pH. This slight aggregation accounts for broader peaks for mostly dispersed viruses at

70–80 nm. We analyze further these observations in terms of protein charge and aggregation state after presenting the effects of surfactants on VLP interactions.

Norovirus integrity and aggregation in the presence of nonionic, cationic, and anionic surfactants

The behavior of VLPs at varying concentrations of added nonionic surfactant, Tween 20, is shown in Fig. 2. The nonionic surfactant shows little impact on the state of the virus in suspension. A peak indicating the presence of dispersed VLPs exists for each concentration used, and no significant amounts of aggregated VLPs are present. A peak indicating the presence of a micelle or capsid protein dimer emerges at all Tween 20 concentrations greater than 0.05%. However the addition of cationic surfactant, CTAB, had a large effect on VLP behavior, stability, and integrity as shown by the DLS data in Fig. 3. These data indicate much more vigorous and diverse effects induced by this surfactant. Peaks representing particle aggregates are present at all concentrations below 0.5%, and peaks indicating the presence of surfactant micelles and/or capsid protein dimers are observed at all concentrations above 0.01%. Peaks representing dispersed viruses are observed at intermediate CTAB concentrations of 0.05% and 0.1%. Finally, the data for VLP behavior in the presence of varying concentrations of the anionic surfactant, SDS, are plotted in Fig. 4. Peaks representing the dispersed virus are present at all concentrations below 0.5%, and micelle or capsid protein dimer peaks are present at all concentrations above 0.01%. Significant aggregate peaks appear at concentrations of 0.05% and 0.1%, which reduce to a small aggregate peak at 0.5%.

These data reveal multiple mechanisms behind the action of these surfactants on the virus dispersions. Norovirus VLPs behave similarly at all concentrations of Tween 20 studied, with a distinct peak representing intact and dispersed particles at each concentration. The critical micelle concentration (CMC) of Tween-20 is 0.005%,[57] and a micelle or protein peak is observed above 0.01%. This discrepancy is probably due to the low concentration of micelles at CMC. The peak of species of diameter < 10 nm most likely represents only surfactant micelles because the peak representing dispersed viruses is present consistently at all concentrations and does not appear to be reduced due to virus loss by capsid disassembly. Even at high concentrations, Tween 20 does not appear to disassemble Norovirus VLPs and may even serve to stabilize them in a well-dispersed, single-virus form.

CTAB has a different effect on VLPs depending on its concentration. Aggregates are present at low concentrations because of heterocoagulation between the surfactant molecules and VLPs. The CMC of CTAB in PBS has been measured at 0.034 wt%.[58] At surfactant concentrations above CMC, we observe the appearance of a peak in intensity indicating the presence of micelles or capsid protein dimers. The disappearance of both dispersed VLP peaks and aggregate peaks at high concentrations of CTAB indicates that this cationic surfactant can disassemble the VLPs above its CMC. This VLP disassembly suggests that CTAB micelles have the ability to disrupt interactions between proteins within the capsid structure and solubilize capsid protein dimers. It is likely that the surfactant molecules assemble around the protein dimers to form a larger micelle-like structure including the dimers. During this de facto solubilization process, the capsid proteins may partially unfold

and reveal more hydrophobic regions. As the concentration of CTAB micelles increases, more VLPs and VLP aggregates are broken apart and solubilized. The appearance of dispersed VLP peaks above CTAB CMC may be attributed to full capsid recharging and electrostatic repulsion between positively charged virus particles with adsorbed CTAB molecules, which we discuss further in the next section.

The anionic surfactant, SDS, also has a distinctly varying effect on VLPs depending on its concentration. SDS adsorption to the capsid surface will increase the apparent magnitude of the VLP net negative surface charge by binding to cationic areas on the surface, which causes increased electrostatic repulsion and dispersion at low concentration. The intensity peaks for particles of large diameter seen at SDS concentrations greater than 0.01% may represent aggregates that form as partially unfolded capsid proteins with exposed hydrophobic regions stick together. The CMC of SDS in pure PBS is about 0.13%,[58] and the peak for particles of diameter 5–10 nm is detected at 0.1% SDS. Therefore this peak most likely represents dimerized proteins from disassembled capsids. VLPs in solution may also alter the CMC of SDS, so micelles may form at lower concentration than in pure PBS. A lower CMC would enable virus disassembly and capsid protein solubilization at a lower SDS concentration than expected.

We observed that the nonionic surfactant, Tween 20, induced VLPs stabilization at all concentrations studied. Many processed food products contain Tween 20 (polysorbate 20) as an emulsifier or stabilizer, so the results lead to the unexpected conclusions that common food additives similar to Tween 20 may actually contribute to the persistence of Noroviruses and perhaps other foodborne viral pathogens. Norovirus VLPs have potential use as vaccines, so these results indicate why nonionic surfactants such as Tween 20 could also be successful candidates for nontoxic vaccine excipients.[27] Conversely, both charged surfactants studied were able to disassemble VLPs at high concentration and solubilize them in surfactant micelles. These strong ionic surfactants are therefore good candidates for virus cleaners and disinfectants. Their differences in behavior at low concentration need to be considered in the context of specific applications and are discussed in more detail in subsequent sections.

Evaluation of the electrostatic interaction contributions to virus dispersion state

The data for the aggregation state of VLPs at varying pH and surfactant concentrations point out that many of the observed effects are a result of the charging of the capsids and their electrostatic interactions in water medium. To interpret the results we evaluated the capsid charge on the basis of its peptide sequence and dissociation properties. The capsid surface charge of the VLPs was calculated based on the number of charged amino acids within the capsid protein and their respective pK_a[59] values using a modification of the Henderson-Hasselbach equation.

$$C_p = -\sum_{iA} n_{iA} \left(1+10^{-(pH-pKa_{iA})}\right)^{-1} + \sum_{iB} n_{iB} \left(1+10^{(pH-pKa_{iB})}\right)^{-1} \quad (1)$$

In eqn (1), the summation in the first term is done over the number of negatively charged residues of different types, n_{iA}, and the second term accounts for the sum of the pH-dependent positively charged residues, n_{iB}. The pH at which this charge equals zero is the theoretical isoelectric point (pI) for the virus capsid. Above the pI, the capsid has a net negative charge due to a higher number of negatively charged amino acids, and below the pI the capsid has a net positive charge due to a higher number of positively charged amino acids. The above formula provides a reasonable estimate of the protein charge and interactions in solution.[40, 59]

Significant changes in surface charge of proteins and colloids can be induced by altering the solution pH or adding charged surfactant. The theoretical capsid charge as a function of pH shown in Fig. 5(a) proves that the Norovirus capsids have a net negative surface charge at low pH, and a net positive surface charge at high pH. This theoretical capsid charge curve predicts that the isoelectric point of the major capsid protein is around 4.5. We see a similar trend in the calculated capsid charge, which is determined from measured zeta potential and also shown in Fig. 5(a). We converted zeta potential to capsid charge using the Grahame equation,[53]

$$\sigma^2 = 2\varepsilon_0 \varepsilon kT\left(\sum\nolimits_i \rho_{0i} - \sum\nolimits_i \rho_{\infty i}\right) \quad (2)$$

where σ is the surface charge density, ε_0 represents vacuum permittivity, ε represents the relative permittivity of water, k is the Boltzmann constant, T the temperature, and ρ_i represents the ion density. Ion density is defined by a Boltzmann distribution,[53]

$$\rho_{0i} = \rho_{\infty i} e^{\frac{-z_i e \psi_0}{kT}} \quad (3)$$

where ρ_{0i} represents the density of ion i at the VLP surface, $\rho_{\infty i}$ represents the density of ion i in the bulk liquid, z_i represents the valence of ion i, e represents the electron charge, and ψ_0 represents the VLP surface potential. The zeta potential equals the surface potential when the slipping plane is located at the particle surface, but this potential is often used as an approximation of surface potential as it can be easily measured.[60] For simplicity and because we are mainly interested in trends in surface charge as a function of pH and surfactant concentration, we approximated the VLP surface potential in eqn (3) with the measured zeta potential. These data suggest that the isoelectric point of the VLPs is about 4.9. Calculated and theoretical capsid charges differ by approximately an order of magnitude likely due to assumptions in the model that the surfaces of the particles are hard spheres. Norovirus particles have protrusions and are slightly porous, so they will not precisely follow DLVO theory. Also, theoretical capsid charge is calculated for the entire capsid protein, much of which is not part of the exposed surface, and thus is likely overestimated. By comparing these capsid charge trends with the diameter of particles as a function of pH as shown in Fig. 5(b), it is straightforward to correlate the capsid charge to the VLP aggregation. Net capsid charge is lowest in magnitude, and the measured size is highest

(obviously resulting from virus aggregation) around the isoelectric point. Net capsid charge is highest in magnitude, and the measured particle size is closest to that of individual VLPs farther away from the isoelectric point. These observations indicate that high capsid charge facilitates electrostatic repulsion between particles that results in dispersed VLPs, and low capsid charge reduces electrostatic repulsion between particles that results in VLP aggregation by van der Waals and hydrophobic attraction. Thus, the VLPs exhibit a behavior common to many colloidal particles and their behavior and stability can be conveniently interpreted on this basis.

We now apply colloidal fundamentals in interpreting how the apparent capsid charge of the VLPs is altered by the addition of charged surfactant. To demonstrate charged surfactant adsorption onto the capsid surface, we measured the zeta potential of VLPs in the presence of different concentrations of CTAB or SDS. We converted this zeta potential into charge density using eqns (2) and (3), then interpreted the difference between the charge density at each surfactant concentration and the charge density without surfactant as the number of charges that were added as a result of surfactant adsorption. Surfactant molecules that adsorb could add a charge or neutralize an opposite charge on the capsid. Both mechanisms result in a loss of one net surface charge. Therefore we assumed that each charge added or subtracted corresponds to the adsorption of one surfactant molecule.

The estimated amount of charged surfactant adsorbed onto VLPs as a function of surfactant concentration is shown in Fig. 6. The addition of oppositely-charged surfactant, CTAB, reduces the magnitude of the zeta potential at low concentration. At concentrations higher than about 0.005%, the amount of CTAB adsorbed on the VLPs is high enough to reverse the sign of the apparent capsid zeta potential. We fit the adsorption data of CTAB onto the VLP surfaces with a simple Langmuir-type adsorption isotherm,

$$\Gamma = \Gamma_{max} \frac{k_{ads} C}{1 + k_{ads} C} \quad (4)$$

where Γ represents mass adsorbed per area, Γ_{max} represents mass adsorbed per unit area at saturation, k_{ads} represents the adsorption constant, and C represents the surfactant concentration in the bulk liquid. We used the surface area of a sphere of diameter 35 nm to approximate the available surface area for surfactant adsorption on the capsid. Because CTAB has positive charge and the capsid has a net negative charge at pH 7.2, the magnitude of the surface charge density first decreases with CTAB adsorption, then increases as the surface becomes saturated. These surfactant-induced changes in VLP surface charge could well describe the particle behaviors shown in Fig. 3. The decrease in magnitude of apparent capsid charge at low CTAB concentration explains the presence of large particle aggregates observed in Fig. 3. As the CTAB concentration is increased, we begin to observe the presence of dispersed particles. An increase in magnitude of the effective positive surface charge by more CTAB adsorption likely enables this re-dispersion process.

The charge shift data for SDS plotted in Fig. 6 indicate a much weaker adsorption likely resulting from hydrophobic interactions (as the SDS has the same sign of charge as the

capsid). We used a linear adsorption isotherm (eqn (5)) to model the binding of some SDS molecules onto the VLP surface.

$$\Gamma = \Gamma_{max} k_{ads} C \quad (5)$$

A linear isotherm describes systems where the adsorbent has low affinity for the surface or where the concentration of adsorbent is low. We assumed that the affinity of SDS for the VLP surface is low at pH 7.2 because the capsid already has a net negative surface charge. Due to micellization, SDS concentrations in the bulk liquid may never become high enough to reach high surface adsorption density. Even low SDS adsorption to the VLP surface causes an increase in magnitude of apparent surface charge. Particle dispersion at low SDS concentration shown in Fig. 4 is facilitated by electrostatic repulsion resulting from this increased magnitude of apparent surface charge. Finally, adsorption data for Tween 20 are not included because the addition of nonionic surfactant does not induce a significant change in measured zeta potential and apparent surface charge.

Overall, the data prove that many of the aqueous VLP interactions reported here depend on the apparent surface charge of the virus capsids. As we observed while varying pH variations and adding charged surfactant, virus aggregation tends to occur where the magnitude of surface charge is low, and conversely, virus dispersion is facilitated by a high magnitude of capsid surface charge and resultant electrostatic repulsion. A decrease in magnitude of the apparent surface charge suppresses the electrostatic repulsion between the dispersed virus particles in solution and subsequently enables their aggregation. Surfactant adsorption to the VLP surface can have multiple origins. For charged surfactants, the head group can bind to an opposite charge on the capsid surface. This mode of adsorption implies a fixed number of surfactant binding sites on the capsid at each pH, which will result in charge neutralization at the right (typically very low) surfactant concentration. In addition, for all classes of surfactant, the hydrophobic tail can adsorb to hydrophobic regions on the capsid surface. This type of adsorption does not imply a fixed number of binding sites and will result in additional charges on the surface in the case of charged surfactants. The head groups of all classes of surfactants can also bind to polar regions on the capsid surface, or any combination of these modes of adsorption can occur. We also obtained data on the combined effects of pH and surfactant, which illustrate complex, but expected trends, and are briefly introduced in Figs. S2 and S3 of the Supplementary Information.

We could also observe directly these patterns of VLP behaviors using electron microscopy. TEM images of each type of system mentioned above are shown in Fig. 7. Dispersed VLPs without surfactant are shown in Fig. 7(a), and intact VLPs in the presence of a low concentration of SDS are shown in Fig. 7(b). A low concentration of CTAB induces the formation of large aggregates ranging from about 0.2 to 1 μm in size formed by intact capsids, which are illustrated in Fig 7(c). These aggregates are separated by areas free of any single VLPs. At high SDS concentration VLP disassembly occurs, and intact capsids are no longer distinguishable, as seen in Fig. 7(d). The three potential mechanisms observed after surfactant addition to VLP solutions are summarized in Fig. 8. These mechanisms include

capsid disassembly due to protein dimer solubilization in surfactant micelles, capsid recharging by surfactant adsorption leading to VLP aggregation, and capsid recharging by surfactant adsorption leading to VLP dispersion and possible blocking of binding receptors. We discuss the biological implications of these results in the next section.

General discussion and conclusions

Based on our results evaluating the aggregation state of Norovirus VLPs in the presence of different classes of surfactants, we conclude that positively-charged surfactants at low concentrations reduce the magnitude of the apparent capsid surface charge enough to induce particle aggregation for capsids with a net negative surface charge. Negatively-charged surfactants at low concentrations increase the magnitude of the apparent capsid surface charge and enhance electrostatic repulsion between the particles. As the concentration of charged surfactant is increased beyond its CMC, the micelles can solubilize capsid protein dimers and therefore disassemble the capsid structure. Thus the surfactants are efficient in disrupting the virus structure only above their CMC, an important finding that should be taken into account when formulating virus cleaning and disinfectant systems with surfactants. Surfactant micellization results in the ability of strong surfactants to disrupt interactions between virus capsid proteins and solubilize individual proteins or dimers. Mild nonionic surfactants can slightly increase repulsion between particles, reducing aggregation and adsorption to surfaces. As mild nonionic surfactants are commonly used in stabilizing food and drink products, our data suggest that their addition to such products may have the undesired potential consequence of stabilizing virus contaminants as well.

The insights on colloidal stability of viruses may also have importance to understanding their biological activity (Fig. 8). We hypothesize that the changes in the virus charge and aggregation could have a profound effect on virus infectivity. Virus particle disassembly by surfactant is likely to lead to complete loss of infectivity, which can also be severely disrupted by the dramatic apparent surface charge alteration and aggregation caused by ionic surfactant. Low concentrations of ionic surfactants (below CMC) are likely to disrupt the virus infectivity much less, while low to moderate amounts of mild nonionic surfactants such as Tween 20 are even likely to enhance virus dispersivity, while potentially increasing their infectivity to some extent. It should be noted, however, that the data reported here are obtained with reconstituted virus capsids, which are likely to be less stable than the native RNA-containing virus assemblies. While the charge and aggregation state of real Noroviruses are likely to be similar to the ones reported here, the natural virus particles may be more stable against surfactant-driven disassembly, contributing to the notoriously large ability for Norovirus to withstand cleanup and disinfection efforts.

The colloidal behavior of Norovirus revealed here should be considered when formulating disinfectants and cleaning agents. The types and concentrations of surfactants used to enhance rinsing of produce should be evaluated with regards to their CMC to determine the optimum concentration for a dispersion state that promotes effective Norovirus clearing. Dispersion state can also influence disinfectant efficiency, so surfactant selection based on colloidal interactions is important in maximizing the accessibility of virucides to virus particles. Capsid recharging by surfactants is also important in evaluating the effectiveness

of water membrane filtration processes. Surfactant adsorption may enhance the long-range dispersion of Noroviruses by protecting them from damage through the reversible formation of aggregates or enhancing particle stability through increased dispersion.

Overall, the characterization of the colloidal interactions, dispersion state, and integrity of the virus particles may provide valuable data in understanding pathogenicity trends and aiding in the development of strategies to prevent virus spread. Characterizing Norovirus behavior is especially important due to its unique resiliency in many different chemical environments. It appears that simple adjustments in the pH, salt conditions, and addition of common surfactants to cleaning and antiviral products can assist in preventing outbreaks and treating Norovirus as an infectious agent.

Experimental

VLPs and surfactants

All experiments were carried out with Houston Norovirus VLPs from genogroup GII.4. The VLPs were provided courtesy of R. Atmar (Baylor College of Medicine, Houston, TX). Sodium dodecyl sulfate (SDS, Sigma Aldrich), cetyltrimethylammonium bromide (CTAB, Sigma Aldrich, St. Louis, MO), and Tween 20 (Sigma Aldrich, St. Louis, MO) were used as surfactant additives. Unless otherwise indicated, all experiments were performed in 0.01 M PBS prepared by adding a PBS tablet (Sigma Aldrich, St. Louis, MO) to deionized water. pH adjustments were achieved by adding small aliquots of 0.1 M sodium hydroxide (Fisher Scientific, Pittsburgh, PA) or hydrochloric acid (Acros Chemical, Pittsburgh, PA).

TEM Images

For viewing under TEM, 100 μg ml^{-1} Norovirus VLPs in 0.15 M NaCl (Sigma Aldrich, St. Louis, MO) containing various surfactant concentrations were adsorbed onto nickel grids with a carbon support film (Ladd Research, Williston, VT). A droplet of VLP solution was applied to each grid for 2 minutes to allow for adsorption. Excess liquid was then removed, followed by 5–10 seconds of negative staining with 2% uranyl acetate. For the images in Fig. 7, the grid-mounted samples were imaged by field emission TEM using a 2010F S/TEM (JEOL, Tokyo, Japan) at 200 kV. For the images in Fig. 8, the grids were imaged by conventional TEM using a 2000FX S/TEM (JEOL, Tokyo, Japan) at 200 kV.

DLS measurements

Protein, micelle, VLP, and aggregate sizes were determined by DLS. VLPs were added to small volume cuvettes (40–70 ul) containing various surfactant concentrations in PBS to a final VLP concentration of 10 μg ml^{-1}. After 30 minutes incubation at room temperature, each sample was measured in triplicate using a Zetasizer Nano ZS (Malvern Instruments) with a 10 mW He-Ne laser at 633 nm and a photodiode located 173° from the incident laser beam. Zetasizer software calculated a size distribution of particles in each sample from light scattering intensity data. Representative graphs of these size distributions for each surfactant conditions are presented. At least 3 replicates of measurements at each surfactant condition were obtained.

Using the CMC and aggregation number[61] of each surfactant and eqn (6), we calculated the number of micelles at each surfactant concentration:

$$M = \frac{C_s - CMC}{N} \quad (6)$$

where M = micelle concentration, C_s = total molar surfactant concentration, CMC = critical micelle concentration, and N = aggregation number. We then compared the relative signal that would be produced by volume and intensity distributions from micelles and VLPs using their respective diameters and concentrations in eqn (7) and eqn (8):

$$R_V = \frac{d_m^3}{d_{VLP}^3} * \frac{M}{C_{VLP}} \quad (7)$$

$$R_I = \frac{d_m^6}{d_{VLP}^6} * \frac{M}{C_{VLP}} \quad (8)$$

where R_V = micelle to VLP ratio of signal from a volume distribution, d_m = diameter of a micelle, d_{VLP} = diameter of a VLP, C_{VLP} = molar VLP concentration, and R_I = micelle to VLP ratio of signal from an intensity distribution. We then related the ratios of concentrations and scattering signals for micelles and VLPs. For each surfactant, $R_I \leq 1$ and $R_V > 1$. Based on these calculations, an intensity distribution expresses VLP behavior more accurately than a volume distribution because micelles scatter as much or less light than VLPs at each concentration.

Zeta potential measurements

VLP electrophoretic mobility was determined by a Zetasizer Nano ZSP (Malvern Instruments) with a 10 mW HeNe laser at 633 nm and a photodiode located 173° from the incident laser beam. Zetasizer software calculated zeta potential from electrophoretic mobility using the Smoluchowski formula. The Smoluchowski formula was assumed to be a reasonable approximation because the Debye length in 0.01 M PBS is 0.76 nm, which is about 50-fold smaller than the VLP radius. VLPs were placed into a glass cuvette containing PBS solutions of varying pH or surfactant concentration to a final concentration of 5 μg ml^{-1} and immediately measured to determine zeta potential before significant aggregation occurred. 0.1 M hydrochloric acid and sodium hydroxide were used for pH adjustments. Each sample was measured in triplicate.

Supplementary Material

Refer to Web version on PubMed Central for supplementary material.

Acknowledgments

The authors acknowledge funding from the USDA-NIFA Food Virology Collaborative (NoroCORE), supported by the National Institute of Food and Agriculture, U.S. Department of Agriculture, under award number 2011-68003-30395. We also thank the Molecular Biotechnology Training Program (MBTP) sponsored by the National Institutes of Health and the Graduate School at North Carolina State University (5 T32 GM008776-15). The authors acknowledge the use of the Analytical Instrumentation Facility (AIF) at North Carolina State University, which is supported by the State of North Carolina and the NSF and the use of the Zetasizer Nano ZSP, which was purchased by the NSF Triangle Materials Research Science and Engineering Center (NSF DMR-1121107).

References

1. Pinto F, Maillard J, Denyer SP. Am J Infect Control. 2010; 38:393–398. [PubMed: 20006410]
2. Hartmann, EM.; Halden, RU. Detection of biological agents for the prevention of bioterrorism. Banoub, J., editor. Springer; Dordrecht, The Netherlands: 2011. p. 158
3. Prasad BVV, Rothnagel R, Jiang X, Estes MK. J Virol. 1994; 68:5117–5125. [PubMed: 8035511]
4. Choi J, Hutson AM, Estes MK, Prasad BVV. Proc Natl Acad Sci U S A. 2008; 105:9175–9180. [PubMed: 18599458]
5. Xagoraraki I, Yin Z, Svambayev Z. J Environ Eng. 2014; 140:04014020.
6. Seo K, Lee JE, Lim MY, Ko G. J Food Prot. 2012; 75:533–540. [PubMed: 22410228]
7. Escudero BI, Rawsthorne H, Gensel C, Jaykus LA. J Food Prot. 2012; 75:927–935. [PubMed: 22564943]
8. Liu P, Yuen Y, Hsiao H, Jaykus L, Moe C. Appl Environ Microbiol. 2010; 76:394–399. [PubMed: 19933337]
9. Nowak P, Topping JR, Fotheringham V, Gallimore CI, Gray JJ, Iturriza-Gomara M, Knight AI. J Virol Methods. 2011; 174:7–11. [PubMed: 21414362]
10. Park GW, Barclay L, Macinga D, Charbonneau D, Pettigrew CA, Vinje J. J Food Prot. 2010; 73:2232–2238. [PubMed: 21219741]
11. Tung G, Macinga D, Arbogast J, Jaykus L. J Food Prot. 2013; 76:1210–1217. [PubMed: 23834796]
12. Whitehead K, McCue KA. Am J Infect Control. 2010; 38:26–30. [PubMed: 19616346]
13. Mattle MJ, Crouzy B, Brennecke M, Wigginton KR, Perona P, Kohn T. Environ Sci Technol. 2011; 45:7710–7717. [PubMed: 21819042]
14. Mattle MJ, Kohn T. Environ Sci Technol. 2012; 46:10022–10030. DOI: 10.1021/es302058v [PubMed: 22913402]
15. Langlet J, Gaboriaud F, Duval JFL, Gantzer C. Water Res. 2008; 42:2769–2777. [PubMed: 18329685]
16. Mylon SE, Rinciog CI, Schmidt N, Gutierrez L, Wong GCL, Nguyen TH. Langmuir. 2010; 26:1035–1042. [PubMed: 19775143]
17. Redman J, Grant S, Olson T, Hardy M, Estes M. Environ Sci Technol. 1997; 31:3378–3383.
18. Wong K, Mukherjee B, Kahler AM, Zepp R, Molina M. Environ Sci Technol. 2012; 46:11145–11153. [PubMed: 22950445]
19. Panyukov YV, Nemykh MA, Dobrov EN, Drachev VA. Macromol Biosci. 2008; 8:199–209. [PubMed: 17886326]
20. Panyukov Y, Nemykh M, Rafikova E, Kurganov B, Yaguzhinsky L, Arutyunyan A, Drachev V, Dobrov E. Int J Biochem Cell Biol. 2006; 38:533–543. [PubMed: 16318921]
21. Predmore A, Li J. Appl Environ Microbiol. 2011; 77:4829–4838. [PubMed: 21622782]
22. Zeltins A. Mol Biotechnol. 2013; 53:92–107. [PubMed: 23001867]
23. Ausar SF, Foubert TR, Hudson MH, Vedvick TS, Middaugh CR. J Biol Chem. 2006; 281:19478–19488. [PubMed: 16675449]
24. Dika C, Duval JFL, Ly-Chatain HM, Merlin C, Gantzer C. Appl Environ Microbiol. 2011; 77:4939–4948. [PubMed: 21622784]

25. Dika C, Gantzer C, Perrin A, Duval JFL. Phys Chem Chem Phys. 2013; 15:5691–5700. [PubMed: 23474807]
26. Nguyen TH, Easter N, Gutierrez L, Huyett L, Defnet E, Mylon SE, Ferri JK, Ai Viet Nguyen. Soft Matter. 2011; 7:10449–10456.
27. Kissmann J, Ausar SF, Foubert TR, Brock J, Switzer MH, Detzi EJ, Vedvick TS, Middaugh CR. J Pharm Sci. 2008; 97:4208–4218. [PubMed: 18300304]
28. Shi L, Sanyal G, Ni A, Luo Z, Doshna S, Wang B, Graham T, Wang N, Volkin D. J Pharm Sci. 2005; 94:1538–1551. [PubMed: 15929070]
29. Cuellar JL, Meinhoevel F, Hoehne M, Donath E. J Gen Virol. 2010; 91:2449–2456. [PubMed: 20592107]
30. da Silva AK, Kavanagh OV, Estes MK, Elimelech M. Environ Sci Technol. 2011; 45:520–526. [PubMed: 21121659]
31. Shoemaker GK, van Duijn E, Crawford SE, Uetrecht C, Baclayon M, Roos WH, Wuite GJL, Estes MK, Prasad BVV, Heck AJR. Mol Cell Proteomics. 2010; 9:1742–1751. [PubMed: 20418222]
32. Uetrecht C, Barbu IM, Shoemaker GK, van Duijn E, Heck AJR. Nature Chemistry. 2011; 3:126–132.
33. Vandenbossche G. Microbiol Res. 1994; 149:105–114. [PubMed: 7921892]
34. Tresset G, Le Coeur C, Bryche J, Tatou M, Zeghal M, Charpilienne A, Poncet D, Constantin D, Bressanelli S. J Am Chem Soc. 2013; 135:15373–15381. [PubMed: 23822934]
35. Prasad BVV, Hardy ME, Dokland T, Bella J, Rossmann MG, Estes MK. Science. 1999; 286:287–290. [PubMed: 10514371]
36. Baclayon M, Shoemaker GK, Uetrecht C, Crawford SE, Estes MK, Prasad BVV, Heck AJR, Wuite GJL, Roos WH. Nano Letters. 2011; 11:4865–4869. [PubMed: 21967663]
37. Leckband D. Annu Rev Biophys Biomol Struct. 2000; 29:1–26. [PubMed: 10940241]
38. Gitlin I, Carbeck JD, Whitesides GM. Angew Chem Int Ed. 2006; 45:3022–3060.
39. Sigstam T, Gannon G, Cascella M, Pecson BM, Wigginton KR, Kohn T. Appl Environ Microbiol. 2013; 79:3455–3467. [PubMed: 23542618]
40. Velev OD, Kaler EW, Lenhoff AM. Biophys J. 1998; 75:2682–2697. [PubMed: 9826592]
41. Velev OD, Nikolov AD, Denkov ND, Doxastakis G, Kiosseoglu V, Stalidis G. Food Hydrocoll. 1993; 7:55–71.
42. Saluja A, Kalonia DS. Int J Pharm. 2008; 358:1–15. [PubMed: 18485634]
43. Kamerzell TJ, Esfandiary R, Joshi SB, Middaugh CR, Volkin DB. Adv Drug Deliv Rev. 2011; 63:1118–1159. [PubMed: 21855584]
44. Wang W, Nema S, Teagarden D. Int J Pharm. 2010; 390:89–99. [PubMed: 20188160]
45. Duval JFL, Gaboriaud F. Curr Opin Colloid Interface Sci. 2010; 15:184–195.
46. Ohshima H. Curr Opin Colloid Interface Sci. 2013; 18:73–82.
47. Langlet J, Gaboriaud F, Gantzer C, Duval JFL. Biophys J. 2008; 94:3293–3312. [PubMed: 18192368]
48. Toropova K, Basnak G, Twarock R, Stockley PG, Ranson NA. J Mol Biol. 2008; 375:824–836. [PubMed: 18048058]
49. White M, Kingma P, Tecle T, Kacak N, Linders B, Heuser J, Crouch E, Hartshorn K. J Immunol. 2008; 181:7936–7943. [PubMed: 19017984]
50. Xiu-ying, Pu; Yu, Liu; Yan, Li; Wei-jie, Zhang; Heng-rui, Wang. Zhongguo Yaolixue Yu Dulixue Zazhi. 2013; 27:187–192.
51. Turro NJ, Lei XG, Ananthapadmanabhan KP, Aronson M. Langmuir. 1995; 11:2525–2533.
52. Otzen D. Biophys J. 2002; 83:2219–2230 ER. [PubMed: 12324439]
53. Israelachvili, JN. Intermolecular and Surfaces Forces, Third Edition. Elsevier Inc; Waltham, MA: 2011. p. 503-534.
54. Skoglund S, Lowe TA, Hedberg J, Blomberg E, Wallinder IO, Wold S, Lundin M. Langmuir. 2013; 29:8882–91. [PubMed: 23758058]
55. Moren A, Khan A. Langmuir. 1998; 14:6818–6826.

56. Larsson MM, Rydell GEP, Rodriguez-Diaz J, Akerlind B, Hutson AM, Estes MK, Larson G, Svensson L. J Infect Dis. 2006; 194:1422–1427. [PubMed: 17054072]

57. Patist A, Bhagwat SS, Penfield KW, Aikens P, Shah DO. J Surfactants Deterg. 2000; 3:53–58.

58. De Paula R, da Hora Machado AE, de Miranda JA. J Photochem Photobiol A. 2004; 165:109–114.

59. Stryer, L. Biochemistry. W. H. Freeman and Co; New York: 1988.

60. Ohshima, H. Encyclopedia of Surface and Colloid Science, 2004 Update Supplement. Somasundaran, P., editor. Vol. 5. Marcel Dekker, Inc; New York, NY: 2004. p. 302

61. Anachkov SE, Danov KD, Basheva ES, Kralchevsky PA, Ananthapadmanabhan KP. Adv Colloid Interface Sci. 2012; 183–184:55–67.

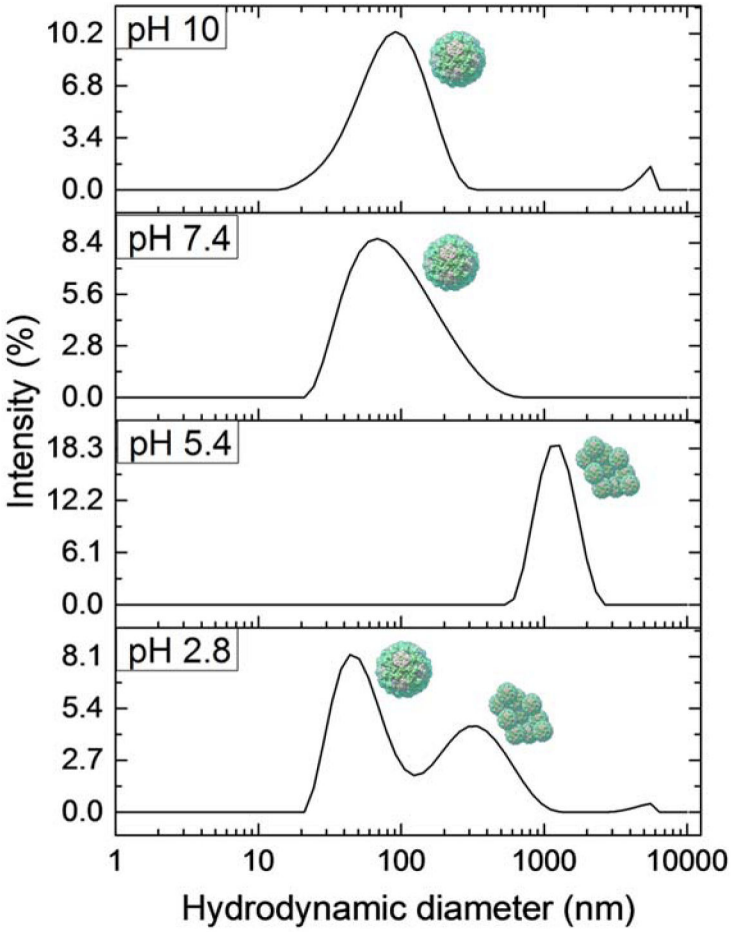

Fig. 1.

Intensity distributions determined by DLS of Norovirus VLPs in PBS of varying pH. The peaks are matched to the schematic presentations of the types of detected species. Data sets are representative curves from 3 repeated measurements for each of 3 different samples at each pH.

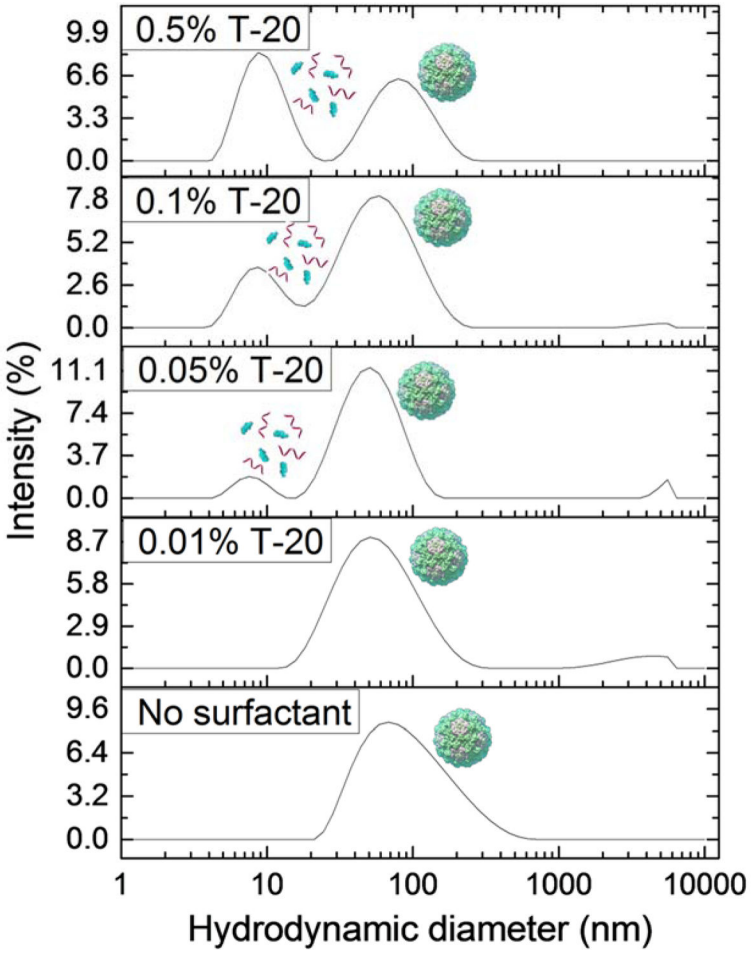

Fig. 2.

Intensity distributions from DLS experiment of Norovirus VLPs in PBS media at pH 7.4 containing 0.01%, 0.05%, 0.1%, and 0.5% Tween 20. The peaks are visually labelled with the schematic presentations of the types of detected species. Data sets are representative curves from 3 repeated measurements for each of 3 different samples at each concentration. The Norovirus VLPs remain stable and well-dispersed at all Tween 20 concentrations tested.

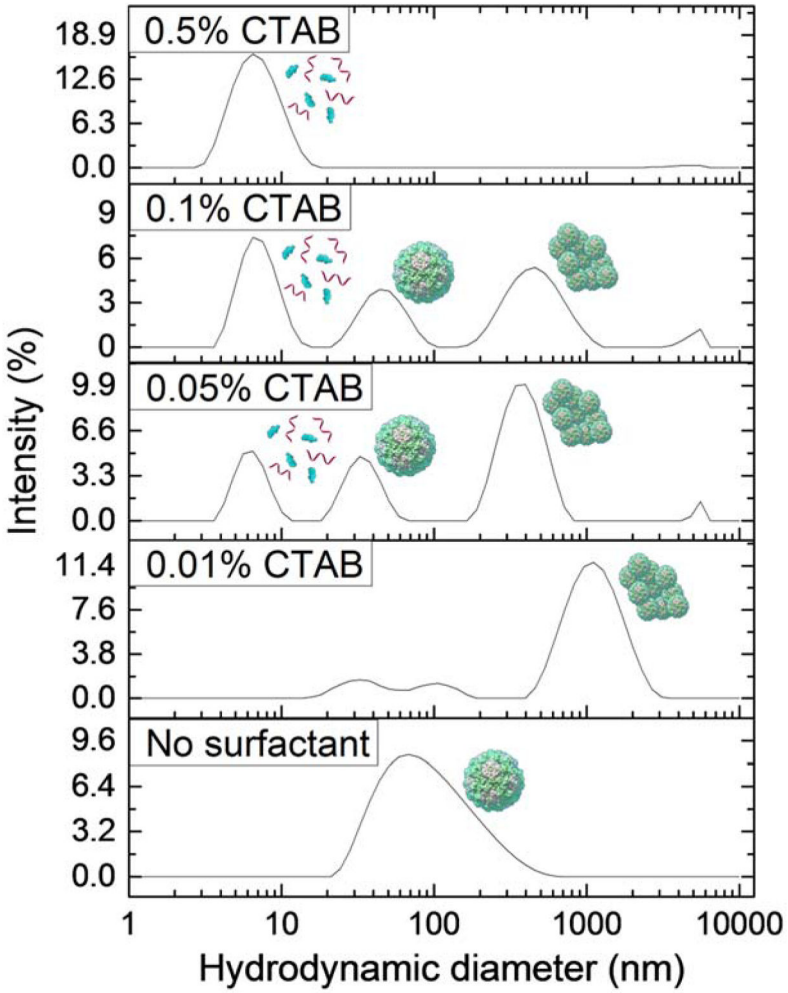

Fig. 3.

Intensity distributions from DLS experiment of Norovirus VLPs in PBS solutions at pH 7.4 containing 0.01%, 0.05%, 0.1%, and 0.5% CTAB. Data sets are representative curves from 3 repeated measurements for each of 3 different samples at each concentration. Norovirus VLPs aggregate in the presence of low concentrations of CTAB and disassemble at high CTAB concentrations.

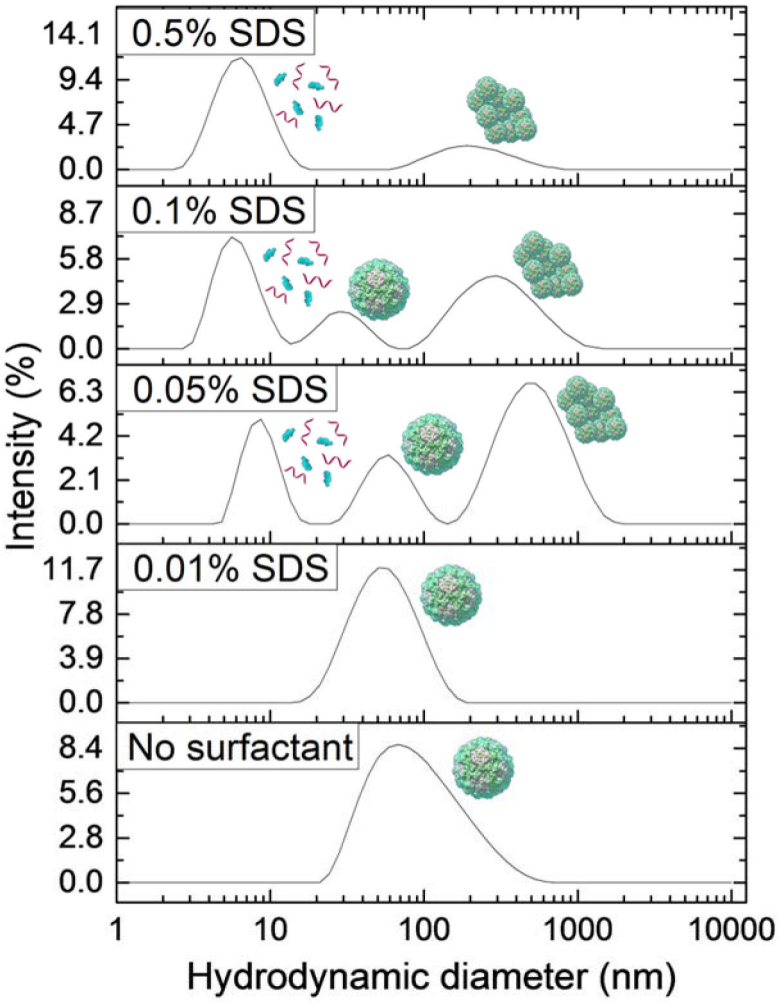

Fig. 4.

Intensity distributions from DLS experiments of Norovirus VLPs in PBS at pH 7.4 containing 0.01%, 0.05%, 0.1%, and 0.5% of anionic surfactant, SDS. The plots are representative data sets from 3 repeated measurements for each of 3 different samples at each concentration. Norovirus VLPs remain dispersed in the presence of low concentrations of SDS, while they first partially aggregate and then disassemble in the presence of high SDS concentrations.

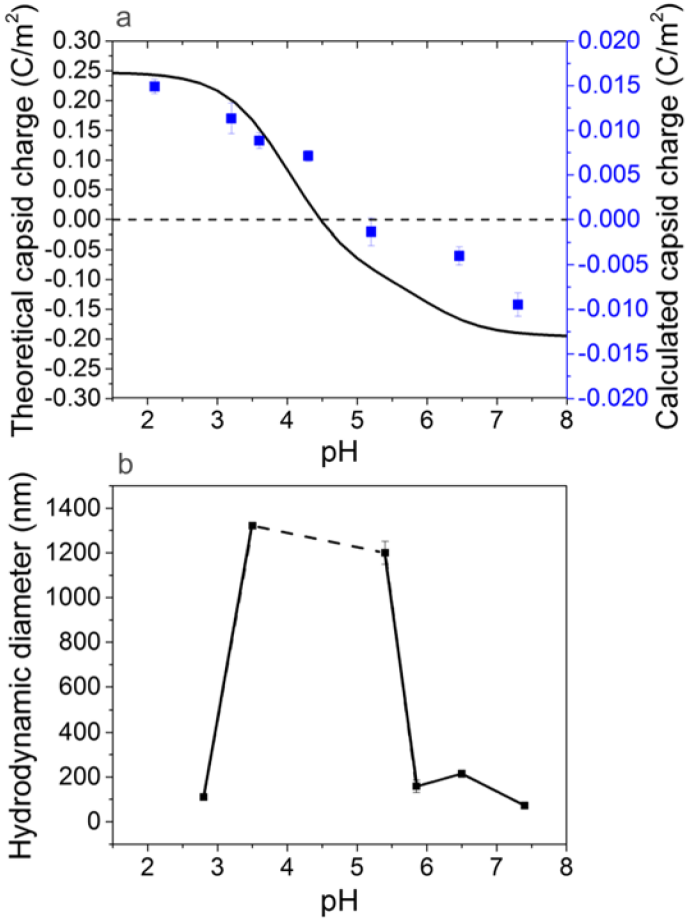

Fig. 5.

Comparison of (a) theoretically evaluated capsid charge (curve) and capsid charge calculated from zeta potential measurements (points) and (b) diameter of VLPs or VLP aggregates at varying pH revealing capsid isoelectric point. The error bars represent the standard error of three measurements at each condition. Theoretical capsid charges at varying pH were calculated using a modification of the Henderson-Hasselbach equation (eqn (1)). There is a very good correlation between the virus capsid surface charge with pH and the aggregation behavior observed by DLS near the isoelectric point.

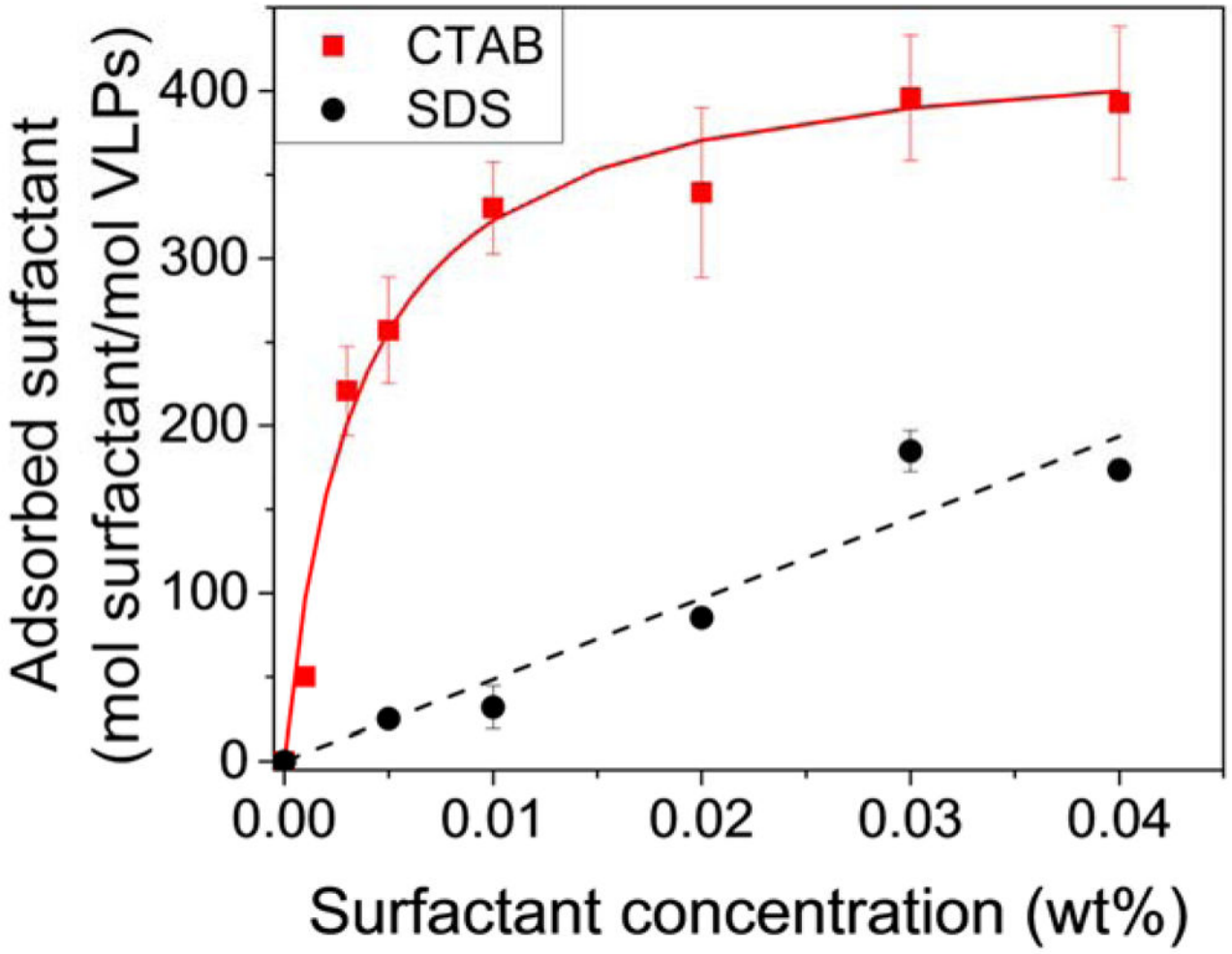

Fig. 6.

Calculated and modeled surfactant adsorption onto VLPs at varying surfactant concentration at pH 7.4. The amount of adsorbed surfactant was calculated by converting the measured zeta potential to charge density with the Grahame equation and then converting the change in charge density to number of surfactant molecules. Error bars represent the standard error of three measurements at each condition. The apparent virus capsid charge can be controlled by adding charged surfactant. Both simple adsorption models interpret adequately the amount of surfactant binding to the model viruses.

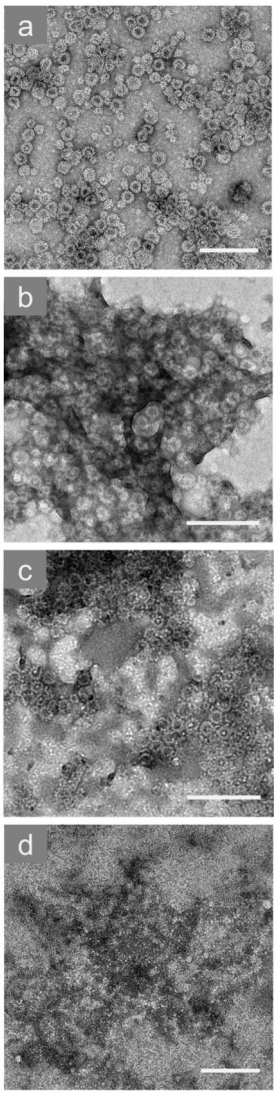

Fig. 7.

TEM images of GII.4 Norovirus VLPs in 0.15 M NaCl, including (a) intact and dispersed capsids without surfactant, (b) intact capsids stabilized by 0.01% SDS, (c) intact capsids aggregated by 0.01% CTAB, and (d) capsids disassembled by 0.5% SDS. The scale bars are equal to 200 nm.

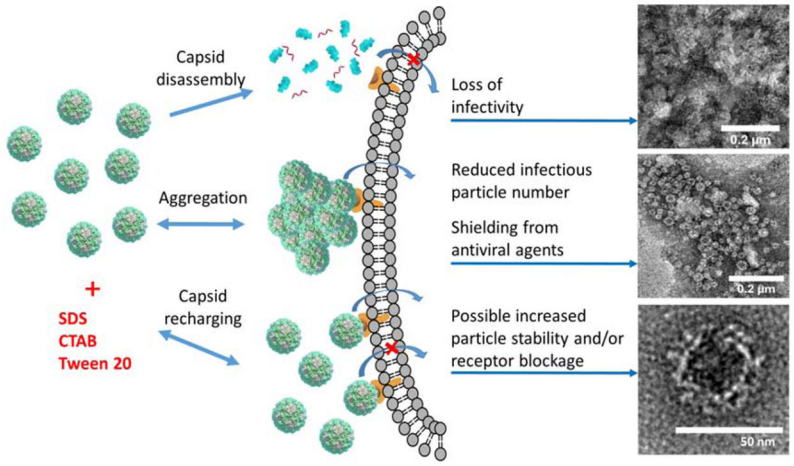

Fig. 8.

Summary of the mechanisms responsible for Norovirus VLP behavior after exposure to three different surfactant types. TEM images represent VLPs stained with uranyl acetate after treatment with 0.5% CTAB (top), 0.01% CTAB (middle), and no surfactant (bottom).